frontiers | Frontiers in Physics

TYPE Original Research
PUBLISHED 24 February 2023
DOI 10.3389/fphy.2023.1153380



OPEN ACCESS

EDITED BY
Leilei Chen,
Huanghuai University, China

REVIEWED BY
Shanju Yang,
Northwest A&F University, China
Lingling Chen,
Northwestern Polytechnical University, China

*CORRESPONDENCE
Chen Xu,
chenxu@whut.edu.cn

SPECIALTY SECTION
This article was submitted to Statistical and Computational Physics, a section of the journal Frontiers in Physics

RECEIVED 29 January 2023
ACCEPTED 14 February 2023
PUBLISHED 24 February 2023

CITATION
Zhao Y, Xu C, Zheng Z, Hu X and Mao Y (2023), Experimental study of the parameter effects on the flow and noise characteristics for a contra-rotating axial fan.
*Front. Phys.* 11:1153380.
doi: 10.3389/fphy.2023.1153380



# Experimental study of the parameter effects on the flow and noise characteristics for a contra-rotating axial fan

Yanjie Zhao[1], Chen Xu[2]*, Zhiwei Zheng[3], Xiaowen Hu[4] and Yijun Mao[1]

[1]School of Aerospace Engineering, Huazhong University of Science and Technology, Wuhan, China, [2]School of Naval Architecture, Ocean and Energy Power Engineering, Wuhan University of Technology, Wuhan, China, [3]Foshan Shunde Midea Washing Appliances Mfg. Co., Ltd., Foshan, China, [4]Corporate Research Center, Midea Group, Foshan, China

**Introduction:** In the present paper, experiments for a contra-rotating axial fan have been conducted to investigate the influences of the fan parameters including axial distance, blade number, blade pattern and blade thickness on the performance and noise characteristics under variable rotational speed regulation.

**Methods:** The characteristic curves and spectrum characteristics of the contra-rotating axial fan with different structural configurations are compared and analyzed. Moreover, the spectrum density of the velocity obtained from the experiment is compared with the classic turbulence models.

**Results:** The results show the characteristic curves of the shaft power and the sound pressure level (SPL) are nearly identical, which indicates the axial distance and blade number are not sensible factors for the contra-rotating axial fan under variable rotational speed regulation. The blade profiles of the fan have an impact on the characteristic curves of the SPL and the shaft power curves of the fan decrease evidently with increase of the blade thickness, while the shaft power curves are very close with different blade patterns.

**Discussion:** In general, the blade profiles are sensible factors for the contra-rotating axial fan under variable rotational speed regulation. Through the SPL spectrum analysis of the contra-rotating axial fan with different blade profile, it can be concluded that the blade profile of the rotors has an obvious impact on the broadband noise characteristics under moderate and high frequency range.

KEYWORDS

**contra-rotating axial fan, acoustic noise, fan configuration, experimental study, spectrum analysis**

**Abbreviations:** BPF, blade passing frequency; SPL, sound pressure level.

# 1 Introduction

Contra-rotating axial fans have been widely applied in the ventilation and air conditioning systems for its merits of the compact size and high pressure rise. Generally, a contra-rotating axial fan is composed of two rotors that rotate in opposite directions with a casing enclosing them. Compared with the traditional fans, the contra-rotating axial fan has the advantage of high efficiency, while with the disadvantage of high noise level. In recent years, many experimental and numerical works have been performed by researchers focusing on contra-rotating fans [1–9].

Compared to fans with a single rotor, the axial spacing of rotors as well as the mounting position for contra-rotating fans has significant impact on the flow and noise characteristics. Roy et al [10] designed a contra-rotating fan unit and tested the flow behavior to improve the performance and to develop an effective design principle. The study found that the contra-rotating unit could enhance the overall stall margins and that at different axial distance between two rotors the performance characteristics varied by 7% at most. In addition, the best performance was observed when the axial distance of two rotors was equal to around 50% of the first rotor chord. Shigemitsu et al [11] developed a high speed contra-rotating axial fan and investigated the performance and the internal flow conditions by experimental and numerical methods. They discussed the influences of the axial distance on the performance and the noise characteristics and illustrated the interaction of the flow field between the rotors. Nouri et al [12] conducted an experimental investigation on the inverse design method of contra-rotating axial fans and the effects of varying the axial distance and rotational speed ratios on the overall performance were analyzed. Mao et al [13] investigated the effects of axial distance on the performance of a contra-rotating axial fan by unsteady numerical simulation. The results suggested that the unsteady effects dominated the flow behavior at smaller axial spacing ranges, while the variation of aerodynamic force for two rotors was different as the axial spacing increased. Sun et al [14] designed a contra-rotating fan for mine ventilation and analyzed the performance and flow characteristics under different speed combinations. The results showed that depending on the flow rate and the resistance of the pipe network, variable speed operation of two rotors expanded the stable working range. In addition, Chen et al [15] conducted experimental and numerical investigations on the performance and detailed flow structure of a contra-rotating fan under different rotational speed ratios. Ravelet et al [16] designed three contra-rotating stages with different rotational speed ratios, mean stagger angles of blades and repartitions of blade loads between two rotors to study the global characteristics and the unsteady features of the flow. Luan et al [17] studied the acoustic and vibration effects of the axial spacing based on the experimental analysis and numerical calculation. Ai et al [18] performed experimental studies on the rotational speed matching of two rotors and analyzed its impact on the stable margin and efficient working range.

As is the case in traditional fans, geometric parameters of the rotor have great impact on the flow and noise in contra-rotating axial fans. Joly et al [19] utilized a multidisciplinary optimization methodology to design a low-weight and high-load contra-rotating fan. Cao et al [20] employed the model of forced vortex and free vortex, in which the real inflow velocity distribution of downstream rotor was considered, to improve the performance and optimize the flow field. Mohammadi et al [21] optimized the blade thickness of a ducted contra-rotating axial flow fan and studied the flow characteristics inside it by numerical simulation. They compared the flow behavior and obtained the characteristic map under the optimum blade thickness. Additionally, the influences of different rotational speed ratios and axial gaps of the contra-rotating fan were also investigated in the paper. Xu et al [22] studied the tip clearance flow and associated loss mechanism of a contra-rotating axial fan and compared the stage efficiency and pressure loss coefficient with different tip clearance based on unsteady numerical simulation. The results indicated that on the same tip clearance variation, the efficiency of the downstream rotor decreased more dramatically than that of the upstream rotor, though the contra-rotating fan efficiency almost linearly changed with tip clearance variation. Wang et al [23] investigated the effects of tip clearance on the performance and found isentropic efficiency and stable operating range decreased with increasing tip clearance size. Furthermore, the negative effect on the performance of the upstream rotor was greater than that of the downstream rotor. Grasso et al [24] presented a multi-objective efficiency-noise optimization approach of the blades of a contra-rotating fan on the basis of artificial neural networks by means of RANS-based hybrid methods that split the description of the flow field from the quantification of the source of noise and of its propagation. Wang et al [25] applied the perforated trailing-edge for the upstream rotor and perforated leading-edge for the downstream rotor of a contra-rotating fan and obtained an overall noise reduction of 6–7 dB with similar aerodynamic characteristics.

Most of the previous investigations on the contra-rotating axial fan focus on the flow and noise characteristics under design point and off-design points at the fixed rotational speed, while in some circumstances, variable rotational speed regulation of the contra-rotating fan is the only practical approach to satisfy the requirement of air quantity. Despite a great deal of research on contra-rotating axial fans, there have been few experimental studies carried out to investigate the influence of the contra-rotating fan parameters on the performance and noise characteristics of the contra-rotating axial fan under variable rotational speed regulation. In the present paper, an experimental study on the performance and noise characteristics of a contra-rotating axial fan under variable rotational speed regulation has been conducted to analyze the influence of the fan parameters. The remainder of this paper is organized as follows. In section 2, the schematics and dimensions of the contra-rotating axial fan model are introduced and the parametric fan configurations are illustrated in detail. Section 3 describes the test rig setup for the contra-rotating fan performance and noise characteristics, as well as the outlet velocity of the main flow region. Section 4 analyzes the tonal noise characteristics of the contra-rotating fan under different rotational speeds and compares the obtained energy spectrum characteristics from experiments with that from classic models. In section 5, the performance and noise characteristics of the contra-rotating axial fan under variable rotational speed regulation are obtained, and on the basis of which the influences of the fan configurations are compared and analyzed. Section 6 draws conclusions.

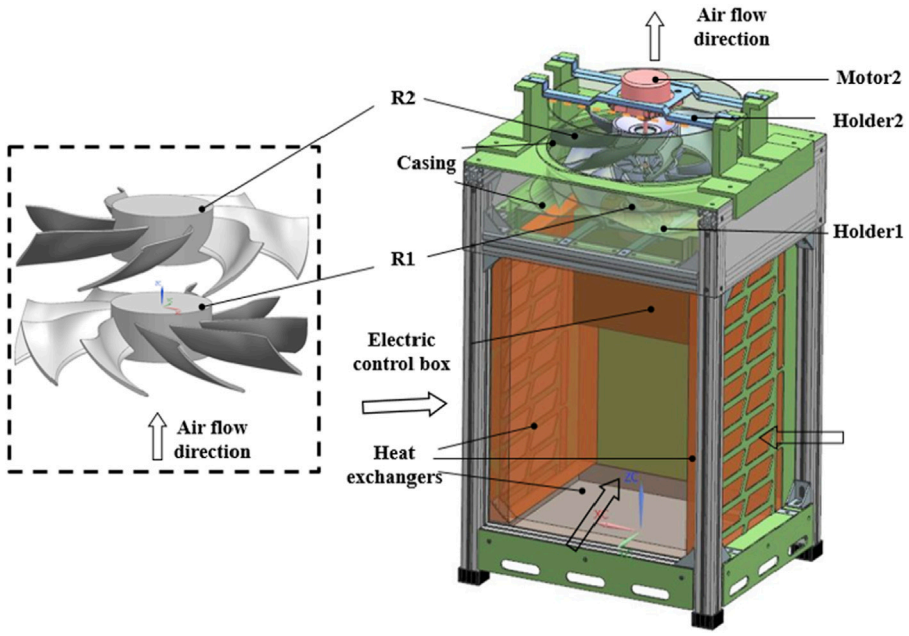


FIGURE 1
Model of the studied contra-rotating axial fan in the apparatus.

# 2 Tested models

## 2.1 The studied contra-rotating axial fan

The present investigation is based on a contra-rotating axial fan installed in the air conditioning system due to the high energy efficiency. Figure 1 illustrates the configuration of the contra-rotation axial fan used in this study, which is applied in an outdoor unit of central air conditioner with an overall dimension of 920 $mm^3$ × 640 $mm^3$ × 600 $mm^3$. The air enters the fan after passing by the three heat exchangers located on the side wall brackets and the electric control box is located on the other side. The air exits from the top side where the axial flow fans are located. The two rotors are fixed by the support brackets and electric motors.

The normal volume flow rate for the outdoor unit is around 2,750 $m^3$/h, and the two rotors rotate at the same speed and to the opposite directions. The diameter of two rotors are 350 mm with a tip clearance of around 5 mm and a hub to tip ratio of 0.35. The tip axial chord length of R2 is slightly smaller than that of R1.

## 2.2 Parametric scheme of contra-rotating axial fan

The contra-rotating axial fan consists of two rotors, and the fan structural parameters such as axial spacing and the blade parameters including the blade number and blade profile have an impact on the performance and noise characteristics.

The axial distance between the upstream rotor and downstream rotor significantly affects the performance and the noise characteristics, as well as the flow field, under the fixed rotational speed [1, 13]. In the present paper, the influence of the axial positions of the two rotors on the performance and noise characteristics of the contra-rotating axial fan under variable rotational speed regulation is also studied. Three schemes with different axial positions of the two rotors are implemented to compare the flow and noise characteristics under variable rotational speed regulation in the experiment. Scheme A represents the original fan with the axial distance of 30 mm. In scheme B, the position of the upstream rotor is fixed and the axial shift of downstream rotor is about 7 mm toward the outlet. In scheme C, the two rotors of the fan are both shifted by 7 mm toward the outlet direction, keeping the axial distance between the two rotors unchanged.

In the present paper, three combinations of blade number for two rotors of the contra-rotating axial fan have been employed to study its influence on the performance and noise characteristics. The scheme 1 is consisted of nine blades for rotor 1 and 7 blades for rotor 2. For scheme 2 and 3, there are both 5 blades for rotor 2, while the blades for rotor 1 respectively are nine and 7.

Apart from the structural parameters of the fan and the rotor, the blade profile such as the blade pattern and thickness, also has a notable impact on the fan performance and noise, as is the case in the rotor-stator blade rows [19, 21]. To study the effect of the blade profile on the flow and noise characteristics of the contra-rotating axial fan, models with three blade pattern and four blade thickness are applied in the present experiment. Figure 2 shows three different distribution models of blade pattern and blade thickness. In the Figure 2, convex, straight and concave represent the three different blade pattern models, and T5, T10, T15, and T20 represent the four blade thickness models.

# 3 Experimental facilities

To study the aerodynamic and noise characteristics of the contra-rotating axial fan, the experimental measurement setups

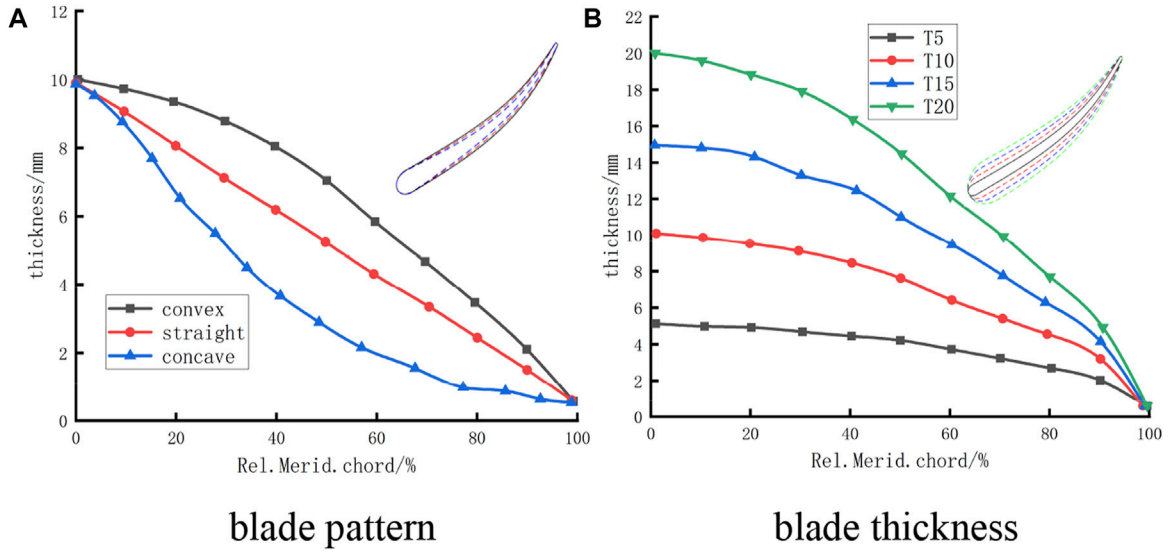


FIGURE 2
Distribution of blade pattern and blade thickness: **(A)** blade pattern; **(B)** blade thickness.

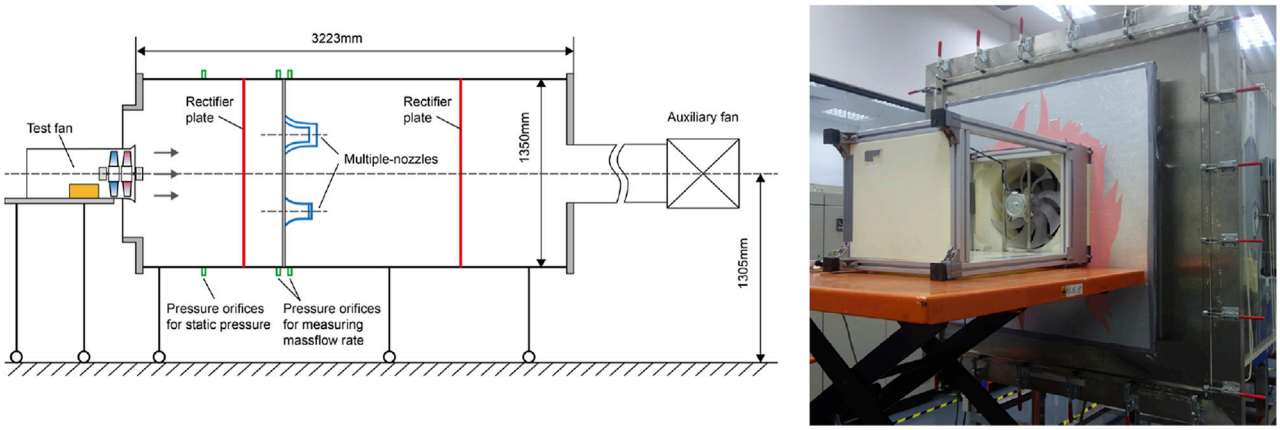


FIGURE 3
Schematic and photograph of the performance test rig.

for the performance and noise characteristics have been performed in Media Corporate Research Center. Besides, the local velocity of the main flow region downstream the outlet of the contra-rotating fan has also been measured to obtain the energy spectrum characteristics of the main flow field.

Figure 3 shows the schematic and photograph of the performance test rig, which has been built according to the Chinese National Standard GB/T7725-2004 and GB/T1236-2000 for the industrial fan performance testing. The volume flow rate which ranges from 500–5,000 $m^3/h$ is calculated according to the pressure difference between the upstream and downstream of the multi-nozzles. The uncertainties of the pressure and airflow rate are 0.15 Pa and 0.004 m3/h, respectively. As shown in Figure 3, the outlet of the contra-rotating axial fan faces toward the test rig, and the three inlet sides of the model should be unobstructed. Pressure orifice 1 is set to measure the static pressure, while pressure orifices 2 and 3 are set to measure the flow rate. The rotational speed of the motor is regulated by a SIMENS MicroMaster frequency converter and measured by a photoelectric digital tachometer. The shaft power is measured by two AC power meters.

The aeroacoustics test has been carried out in a semi-anechoic chamber in Midea Corporate Research Center. The size of the semi-anechoic chamber is 9.6 m long by 5.2 m wide by 3.9 m high and the inside surfaces are lined with mineral wool wedges of 69 cm deep. Figure 4 illustrates the schematic and photograph of the noise test rig, which has been built based on the Chinese National Standard GB/T17758. Four sampling points of

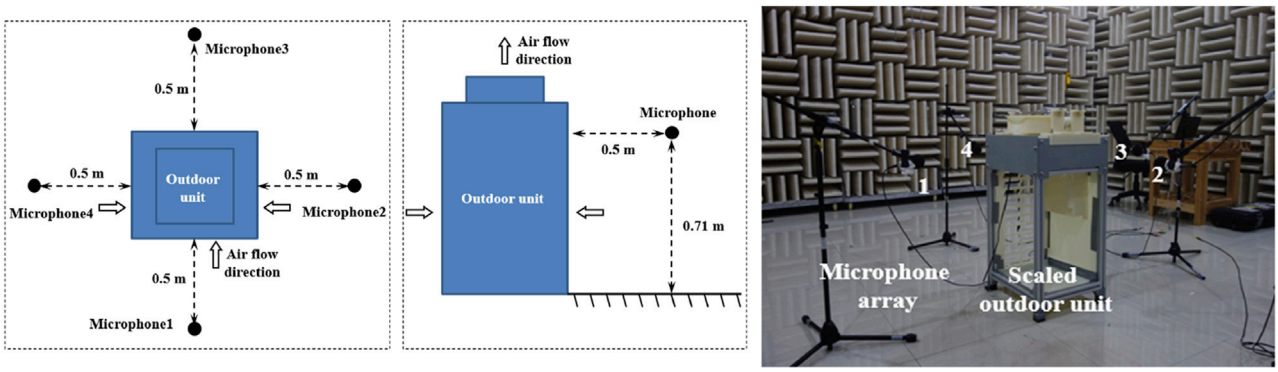


FIGURE 4
Schematic and photograph of the noise test rig.

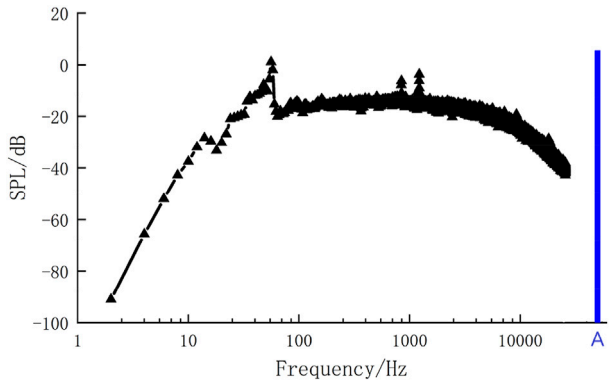


FIGURE 5
SPL spectrum of the background noise.

the noise spectra around the contra-rotating axial fan have been sampled in a semi-anechoic chamber and four microphones are arranged on the four sides of the fan to test the noise characteristics. The height between the measuring points and the ground is 0.71 m, and the distance of the measuring points from the model is 0.5 m.

During the noise test, PCB microphones and preamplifiers, combined with LMS data acquisition system SCADAS Mobile SCM01, are implemented to proceed the measurement and data acquisition of the noise signals. The data acquisition frequency is 10 kHz and the acquisition time is 15 s at each sampling.

To obtain the energy spectrum characteristics of the main flow region downstream the contra-rotating axial fan, the outlet velocity of the main flow field has been measured *via* the hotwire anemometer. The sampling point is located at 50% span of the rotor 2 outlet and 80% of the tip axial chord length downstream the rear rotor trailing edge opposite the side of the electric control box. The acquisition frequency is 32 kHz and the acquisition time is 32 s for the experimental sampling.

# 4 Noise and flow characteristics of the contra-rotating axial fan

## 4.1 Background noise

Figure 5 gives a typical SPL spectrum of the background noise in the hemi-anechoic chamber, and the overall A-weighted SPL of the background noise is around 17.6 dB, which is much lower than the studied fan noise level. In consequence, the effect of the background noise on the noise experiments of the contra-rotating axial fan in the hemi-anechoic chamber in Midea Corporate Research Center is rather negligible.

## 4.2 SPL comparison of four measuring points

As demonstrated in the previous section, four PCB microphones are arranged on the four sides of the fan unit to test the sound pressure level. Table 1 compares the sound pressure levels at four measuring points, and the results indicate that the overall sound pressure levels of the contra-rotating fan are nearly independent of the circumferential angle, thus the noise feature at only one sampling point is analyzed in the following text. Therefore, in the following investigation, the noise data obtained from Microphone1 is applied.

## 4.3 Noise characteristics of the contra-rotating axial fan

The SPL spectra of the model with nine blades for rotor 1 and 7 blades for rotor 2 under different frequencies at different rotational speeds is shown in Figures 6A, B, the frequency is non-dimensionalized by the rotational frequency. It can be seen in Figure 6A, the broadband noise components of the SPL spectra from 100 Hz to 1,000 Hz show the highest value under different rotational speeds. From Figure 6B, the first peak of the SPL under non-dimensional frequency of 1 at different rotational speeds

**TABLE 1** A-weighted SPL of four measuring points at different rotational speeds.

| (rpm) | Mircophone1/0° (dB) | Mircophone2/90° (dB) | Mircophone3/180° (dB) | Mircophone4/270° (dB) |
|---|---|---|---|---|
| 640 | 55.03 | 54.69 | 54.91 | 55.19 |
| 720 | 57.39 | 57.11 | 56.92 | 57.25 |
| 800 | 60.78 | 60.39 | 60.21 | 60.57 |
| 960 | 65.53 | 65.16 | 64.99 | 65.37 |

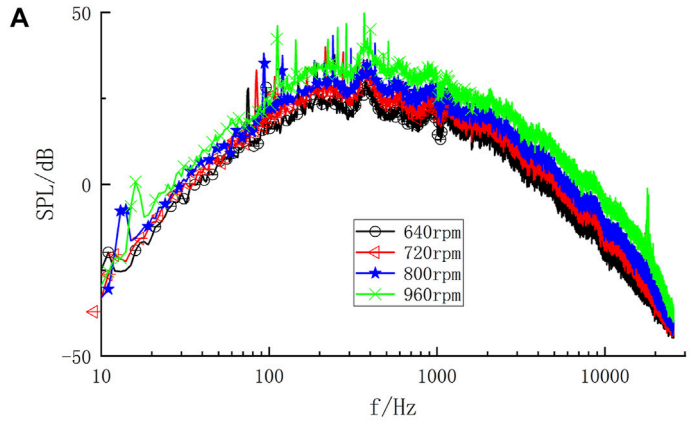


SPL spectrum under different frequencies

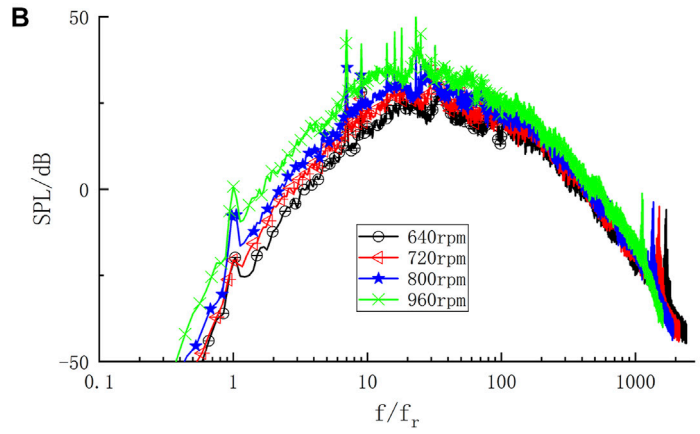


SPL spectrum under nondimensionalized frequencies by the rotational frequency

FIGURE 6
SPL spectrum of the contra-rotating axial fan at different rotational speeds: **(A)** original SPL spectrum; **(B)** nondimensional SPL spectrum.

appears, and the following peaks of the SPL at different rotational speeds all appear under the blade passing frequency of rotor 1 and rotor 2 and their harmonic. It then can be concluded that the primary tonal noise is probably caused by the electric box and by the interaction of two blade rows. It also can be seen that with the increase of the rotational speed of the fan, the tonal noise at the blade passing frequency and its harmonic, as well as the tonal noise at the rotational frequency, becomes higher. Besides, the noise peak value at around 18,000 Hz in Figure 6A is probably generated from the frequency converter, which remains unchanged at different rotational speeds.

Figure 7 shows the non-linear fitting of the tonal SPL for fundamental frequency of rotor 1 and rotor 2 under different rotational speeds. From Figure 7, it can be obtained that the expressions of the fitted curve for fundamental frequency of rotor 1 and rotor 2 are as follows,

$$SPL_{f_{r1}} = 89.95\lg n - 225.8 \quad (1)$$

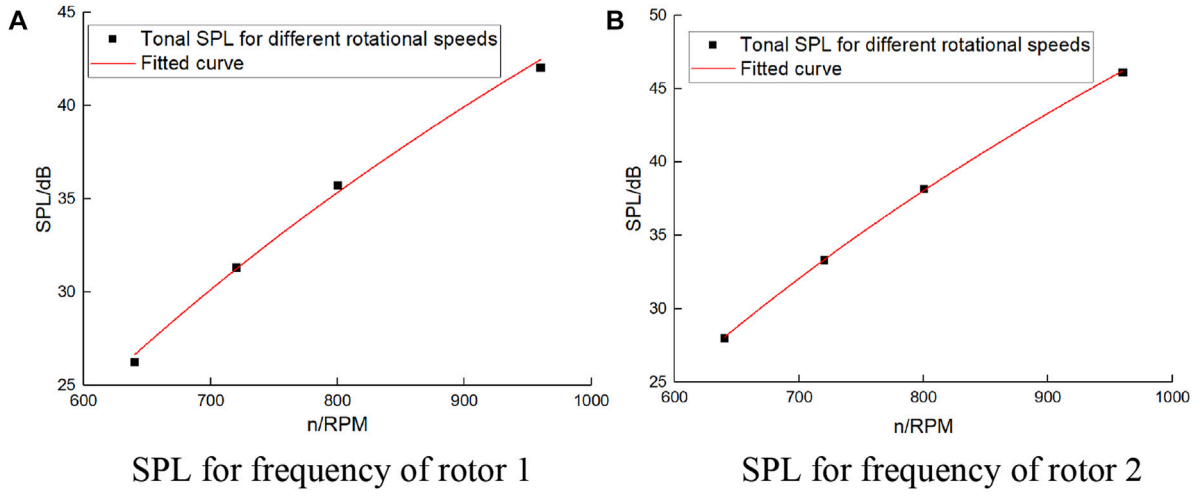


FIGURE 7
Tonal SPL for fundamental frequency of rotor 1 and rotor 2: **(A)** SPL for rotor 1; **(B)** SPL for rotor 2.

$$SPL_{f_{r2}} = 103.05\lg n - 261.09 \tag{2}$$

where $n$ represents the rotational speed of the fan.

The expression of SPL is as following,

$$SPL = 20\lg\frac{P}{P_{ref}} \tag{3}$$

where $P$ represents the sound pressure and $P_{ref}$ represents reference sound pressure, which is $2 \times 10^{-5}$ Pa.

It then can be concluded that

$$P_{f_{r1}} \propto U^{4.55} \tag{4}$$

$$P_{f_{r2}} \propto U^{5.15} \tag{5}$$

where $U$ represents the characteristic velocity and is proportionate to the rotational speed $n$.

With the increase of the rotational speed of the fan, the tonal noise at the blade passing frequency and its harmonic becomes higher, which indicates the interaction of the blade rows grows intense. Based on the analysis above, the SPL of the tonal noise under fundamental frequency of rotor 1 and rotor 2 can be predicted under different rotational speeds.

## 4.4 Flow characteristics of the contra-rotating axial fan

The accuracy of computing the fan broadband noise, in a very large part, relies on the accuracy of the flow characteristics, thus the adequacy of the turbulence model is one of the principal elements for the accurate simulation of broadband noise. The flow in the simulation of the fan is commonly assumed as isotropic turbulence, for which the Liepmann and von Karman models are the most popular models.

The Liepmann model based on the exponential law assumption of turbulence longitudinal correlation coefficient

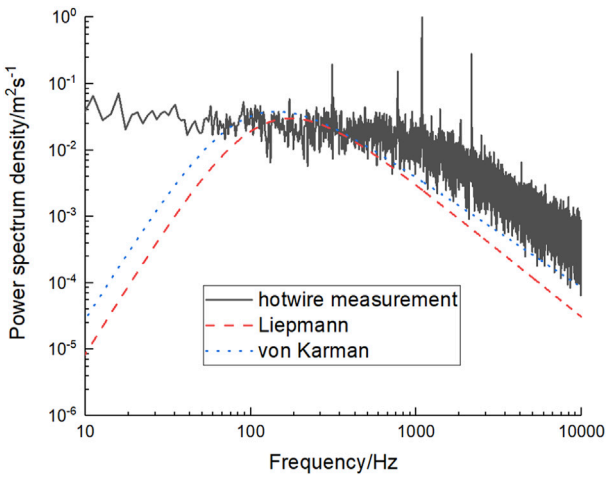


FIGURE 8
Power spectrum density under different models and hotwire measurement.

presents the expression of the three-dimensional energy spectrum as following,

$$E_L(k) = \frac{8u_{rms}^2\Lambda^5}{\pi}\frac{k^4}{\left(1+\Lambda^2k^2\right)^3} \tag{6}$$

where $E(k)$ is the three-dimensional energy spectrum, $k$ represents the wave number and $\Lambda$ represents the turbulence integral scale, and $u_{rms}$ is the root mean square turbulence velocity. For the large eddies with most of the turbulence energy, the Liepmann model shows the law of $k^4$ well, while for the inertial subrange, it shows the law of $k^{-2}$ which has a discrepancy from the −5/3 exponential law presented in experiments.

The von Karman model, which is presented in the following, exhibits similar feature for the range of large eddies, while for the inertial subrange, it shows the −5/3 exponential law.

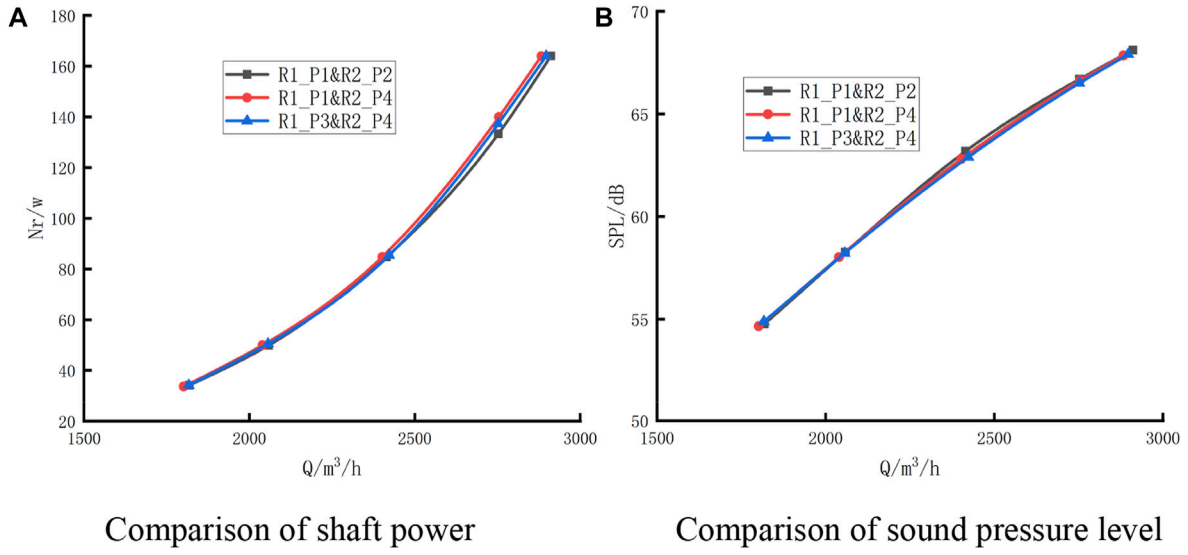


FIGURE 9
Variable rotational speed regulation characteristics of the fan with different axial distances: **(A)** comparison of shaft power; **(B)** comparison of SPL.

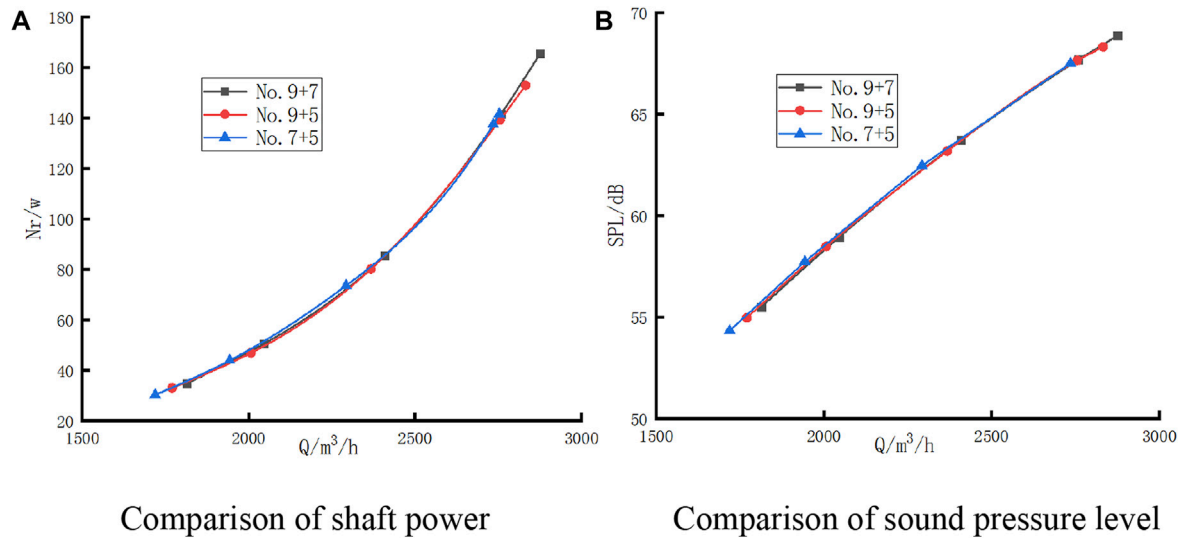


FIGURE 10
Variable rotational speed regulation characteristics of the fan with different blade number combinations: **(A)** comparison of shaft power; **(B)** comparison of SPL.

$$E_v(k) = \frac{55\Gamma(5/6)}{9\sqrt{\pi}\Gamma(1/3)} u_{rms}^2 \Lambda^5 \left(\frac{\Gamma(1/3)}{\sqrt{\pi}\Gamma(5/6)}\right)^4 \frac{k^4}{\left(1+\left(\frac{\Gamma(1/3)}{\sqrt{\pi}\Gamma(5/6)}\right)^2 \Lambda^2 k^2\right)^{17/6}} \tag{7}$$

where $k$, $u_{rms}$ and $\Lambda$ represent the parameters shown in the Liepmann model.

In order to compare the energy spectrum density of the measured velocity with that of the Liepmann and von Karman models. Figure 8 compares the power spectrum density under the Liepmann and von Karman models with that obtained from hotwire measurement. It then can be seen that for f<<100 Hz, $psd_V(f) = 2.26 psd_L(f)$, and spectral density of the two models largely varies with $f^4$. Meanwhile, the power spectral density of the measured velocity changes slightly for this range of frequency, in which the spectral density obtained from hotwire measurement is apparently higher than that obtained from the two models. This is probably because in the lower frequency range, the scale of vortex is large and the flow is anisotropic turbulence, which leads to significant difference between the experimental results and that obtained from Liepmann and von Karman models. While for 100 Hz < f < 1,000 Hz, the difference between $psd_V(f)$ and $psd_L(f)$ is very small. In this frequency range,

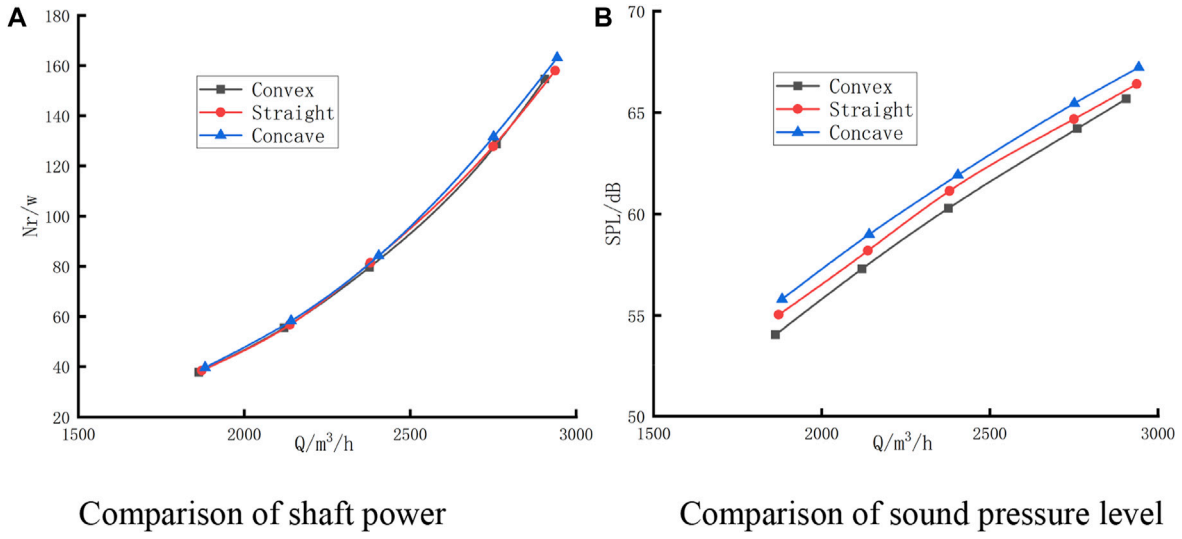


FIGURE 11
Variable rotational speed regulation characteristics of the fan with different blade patterns: **(A)** comparison of shaft power; **(B)** comparison of SPL.

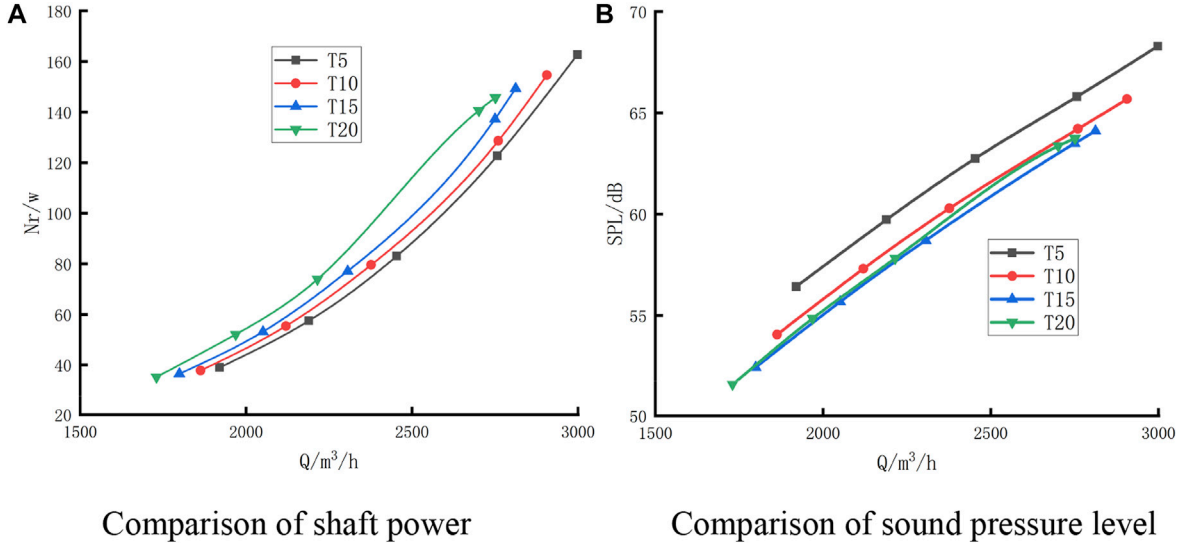


FIGURE 12
Variable rotational speed regulation characteristics of the fan with different blade thicknesses: **(A)** comparison of shaft power; **(B)** comparison of SPL.

the scale of vortex is relatively small and the turbulent flow is approximately local isotropic, thus the experimental results and that obtained from Liepmann and von Karman models agree well. Besides, in this range of frequency, the power spectral density of the measured velocity is pretty close to that obtained from the Liepmann and von Karman models. In addition, the variance of spectral density obtained from the Liepmann and von Karman models gradually increases for f>>1,000 Hz owing to the fact that $psd_L(f)$ decays slightly faster than $psd_V(f)$, and the power spectral density of von Karman model is closer to that of the measured velocity in this range of frequency.

# 5 Influence of the fan parameters on the performance and noise characteristics

## 5.1 Investigation of variable rotational speed regulation characteristics of the fan

Due to the limitation of certain conditions, variable rotational speed regulation of the contra-rotating fan is probably the only practical approach to satisfy the requirement of air quantity. In the present experiment, the

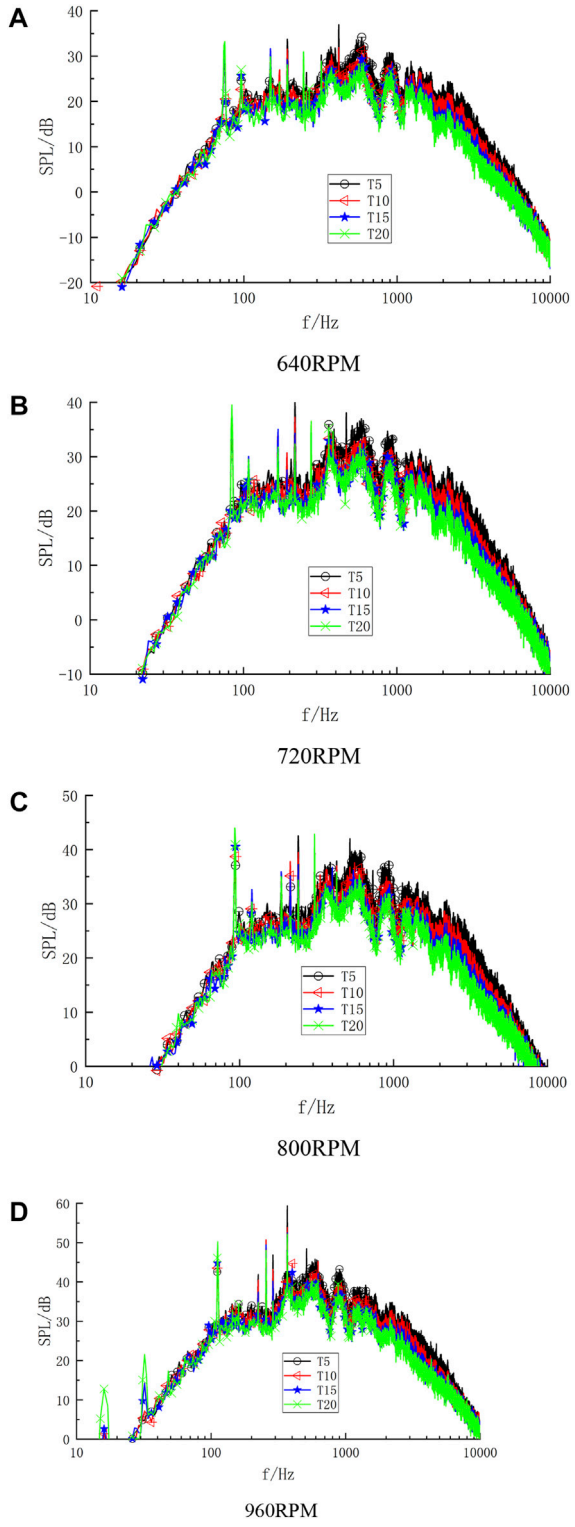


FIGURE 13
SPL spectrum of the contra-rotating axial fan with different blade thicknesses: **(A)** SPL under 640RPM; **(B)** SPL under 720RPM; **(C)** SPL under 800RPM; **(D)** SPL under 960RPM.

performance and noise characteristics under variable rotational speed regulation are obtained to investigate the influences of the fan parameters.

Figure 9 shows variable rotational speed regulation characteristics of the fan with different axial distances. It can be seen that under variable rotational speed regulation, there is remarkably little variation of characteristic curves of shaft power and SPL.

Through the variable rotational speed regulation, the three fan models nearly reach the same volume flow rate. It can be seen that not only the shaft power and SPL are fairly close, but the rotational speed is also basically unchanged at the design point for all of the three models.

Figure 10 shows variable rotational speed regulation characteristics of the fan with different blade number. It can be seen that under variable rotational speed regulation, the characteristic curves of the shaft power and SPL are nearly identical.

It can be seen that the shaft power and SPL of the fan show rather small differences under the three blade number combinations, while there is an increase of the rotational speed with decrease of the blade number.

Figure 11A shows that the shaft power curves of the fan with the three different blade patterns are very close, especially for the cases with straight and concave blade patterns, the characteristic curves of the shaft power are basically identical. For the fan with the three blade patterns, the characteristic curves of SPL under variable rotational speed regulation vary obviously, as shown in Figure 11B, and the convex blade gets the lowest noise level of all three patterns.

It can be seen that near the design flow rate, the fan model with the convex blade pattern shows slightly better performance and noise characteristics. Meanwhile, to achieve the required design flow rate, the rotational speed for the fan models with different blade pattern varies slightly.

Figure 12A shows that the shaft power curves of the fan with the different blade thicknesses under variable rotational speed regulation increase evidently with the increase of the blade thickness. Meanwhile, it can be seen in Figure 12B that with increase of the blade thickness, the SPL curves of the fan decrease evidently first, and with the blade thickness of 15 mm, it shows the lowest noise characteristics. While with the increase of the blade thickness from 15 mm to 20 mm, the SPL curves are quite close. This indicates there might be an optimum blade thickness to get the best noise characteristics.

It can be seen that with the increase of the blade thickness, to reach the flow rate near design point, the required rotational speed and shaft power of the fan model both increase, while the SPL decreases first and then increases slightly. Besides, the disparity of the rotational speed for the fan models with the blade thickness is obviously larger than that for the fan models with the blade pattern.

## 5.2 Spectrum analysis of the fan with different blade profiles

To analyze the influence of the blade thickness on the noise characteristics, Figure 13 shows the SPL spectra of the contra-rotating axial fan with the different blade thicknesses under four different rotational speeds. It can be seen from that below the fundamental frequency of rotor 1 and rotor 2, the SPL varies slightly for the model fan with different blade thicknesses under four different rotational speeds. For the frequencies between 100 Hz

and 5,000 Hz, the broadband noise of the model fan decreases with the increase of the blade thickness, which indicates that the blade thickness has an obvious impact on the band noise of the contra-rotating axial fan in this frequency range. Meanwhile, in this frequency range, the SPL of the broadband noise varies evidently for the model with the blade thickness from 5 mm to 15 mm, compared with that from 15 mm to 20 mm. While for the higher frequency range (f > 5,000 Hz), the influence of the blade thickness on the SPL gradually decreases.

Additionally, the tonal SPL for fundamental frequency of rotor 1 and rotor 2 of the fan slightly increases with the increase of the blade thickness, which is evidently different from the influence of the blade thickness on the broadband components. Moreover, at its harmonic of the BPF, the variation of tonal SPL is inconsistent with that at fundamental frequency for the model fan with different blade thickness.

In general, the broadband noise of the model fan with the different blade thicknesses between 100 Hz and 5,000 Hz is obviously lower than that out of this frequency range (f < 100 Hz or f > 5,000 Hz), and this also applies to the models with the different blade pattern. It then can be concluded that the blade profile of the contra-rotating fan has an obvious impact on the broadband noise characteristics under moderate and high frequencies.

## 6 Conclusion

In the present experimental study, the performance and noise characteristics of a contra-rotating fan under variable rotational speed regulation are studied, and models with different parameters of the fan are applied in the experiments. Compared with the existing experimental and numerical investigations, the present research attempts to discuss the influences of structural and blade parameters of the contra-rotating fan on variable rotational speed regulation characteristics of performance and noise, thus provides instructions for designing contra-rotating axial fans. Conclusions are drawn as follows.

1) It can be concluded that the tonal sound pressure for fundamental frequency of rotor 1 and rotor 2 is proportionate to 4.55th and 5.15th power of the characteristic velocity, respectively, which is proportionate to the rotational speed. For the accurate prediction of flow characteristics which to a great extent determine the accurate prediction of the broadband noise, the Liepmann and von Karman models yield close results for the power spectrum density at moderately high frequencies, where the two models effectively predict the spectrum density of the velocity. It probably because in this frequency range, the scale of vortex is relatively small and the turbulent flow is approximately local isotropic, thus the experimental results and that obtained from Liepmann and von Karman models agree well. While at higher frequencies, the power spectral density of von Karman model, compared with that of Liepmann model, is closer to that of the measured velocity.
2) For the contra-rotating axial fans with different axial distances between rotors or blade number combinations, the characteristic curves of the shaft power and SPL are nearly identical, which indicates the axial distance and blade number are not sensible factors for the contra-rotating axial fan under variable rotational speed regulation. Under variable rotational speed regulation, the blade profiles of the fan, including the blade pattern and thickness, have an impact on the characteristic curves of the SPL. The shaft power curves of the fan with the different blade thicknesses decrease evidently with increase of the blade thickness, while the shaft power curves are very close with different blade patterns. In general, the blade profiles, especially the blade thickness, are sensible factors of the performance and noise characteristics for the contra-rotating axial fan under variable rotational speed regulation.
3) The SPL varies slightly for the model fan with different blade profile below the fundamental frequency of rotor 1 and rotor 2, while the blade profile of the rotors has an obvious impact on the broadband noise characteristics under moderate and high frequency range. Moreover, for the higher frequency range (f >5000 Hz), the influence of the blade thickness on the SPL gradually decreases.

## Data availability statement

The original contributions presented in the study are included in the article/supplementary material, further inquiries can be directed to the corresponding author.

## Author contributions

YZ: writing original draft, data analysis; CX; writing-review and editing; ZZ; software and editing; XH: analysis and reviewing; YM: conceptualization, reviewing and editing.

## Funding

The research is supported by the National Natural Science Foundation of China (No. 52076086).

## Conflict of interest

Authors ZZ was employed by Foshan Shunde Midea Washing Appliances Mfg. Co., Ltd. and XH was employed by Midea Group.

The remaining authors declare that the research was conducted in the absence of any commercial or financial relationships that could be construed as a potential conflict of interest.

## Publisher's note

# References


1. Mistry C, Pradeep AM. Effect of variation in axial spacing and rotor speed combinations on the performance of a high aspect ratio contra-rotating axial fan stage. *P Mech Eng A-j Pow* (2013) 227(2):138–46. doi:10.1177/0957650912467453

2. Mistry C, Pradeep AM. Influence of circumferential inflow distortion on the performance of a low speed, high aspect ratio contra rotating axial fan. *J Turbomach* (2014) 136(7):0710091–11. doi:10.1115/1.4025953

3. Fukutomi J, Shigemitsu T, Yasunobu T. Performance and internal flow of sirocco fan using contra-rotating rotors. *J Therm Sci* (2008) 17(1):35–41. doi:10.1007/s11630-008-0035-8

4. Shigemitsu T, Fukutomi J, Okabe Y. Performance and flow condition of small-sized axial fan and adoption of contra-rotating rotors. *J Therm Sci* (2010) 19(1):1–6. doi:10.1007/s11630-010-0001-0

5. Heinrich M, Khaleghi H, Friebe C. Effect of circumferential casing treatment on low-speed contra-rotating fans. *J Appl Fluid Mech* (2020) 13(6):1719–26. doi:10.47176/JAFM.13.06.31492

6. Dong B, Jiang C, Liu X, Deng Y, Huang L. Theoretical characterization and modal directivity investigation of the interaction noise for a small contra-rotating fan. *Mech Syst Signal Pr* (2020) 135:106362–15. doi:10.1016/j.ymssp.2019.106362

7. Dong B, Xie D, He F, Huang L. Noise attenuation and performance study of a small-sized contra-rotating fan with microperforated casing treatments. *Mech Syst Signal Pr* (2021) 147:107086107086–16. doi:10.1016/j.ymssp.2020.107086

8. Wang C, Huang LX. Theoretical acoustic prediction of the aerodynamic interaction for contra-rotating fans. *AIAA J* (2018) 56(5):1855–66. doi:10.2514/1.j055845

9. Sarraf C, Nouri H, Ravelet F, Bakir F. Experimental study of blade thickness effects on the overall and local performances of a controlled vortex designed axial-flow fan. *Exp Therm Fluid Sci* (2011) 35(4):684–93. doi:10.1016/j.expthermflusci.2011.01.002

10. Roy B, Ravibabu K, Rao PS, Basu S, Raju A, Murthy PN. Flow studies in ducted twin-rotor contra-rotating axial flow fans. In: ASME 1992 International Gas Turbine and Aeroengine Congress and Exposition; June 1–4, 1992; Cologne, Germany (1992). V001T01A131-92-GT-390.

11. Shigemitsu T, Fukutomi J, Okabe Y, Iuchi K, Shimizu H. Unsteady flow condition of contra-rotating small-sized axial fan. *J Therm Sci* (2011) 20(6):495–502. doi:10.1007/s11630-011-0501-6

12. Nouri H, Ravelet F, Bakir F, Sarraf C, Rey R. Design and experimental validation of a ducted counter-rotating axial-flow fans system. *J Fluid Eng-t ASME* (2012) 134(10):104504.1–6. doi:10.1115/1.4007591

13. Mao XC, Liu B. A numerical study on the unsteady effect of axial spacing on the performance in a contra-rotating axial compressor. *P Mech Eng C-j Mec* (2017) 231(14):2598–609. doi:10.1177/0954406216638881

14. Sun XB, Meng DW, Liu BW, Wang Q. Numerical investigation of differential speed operation of two impellers of contra-rotating axial-flow fan. *Adv Mech Eng* (2017) 9(10):168781401772008168781401772008–16. doi:10.1177/1687814017720083

15. Chen YY, Liu B, Xuan Y, Xiang XR. A study of speed ratio affecting the performance of a contra-rotating axial compressor. *P Mech Eng G-j Aer* (2008) 222(G7):985–91. doi:10.1243/09544100jaero364

16. Ravelet F, Bakir F, Sarraf C, Wang J. Experimental investigation on the effect of load distribution on the performances of a counter-rotating axial-flow fan. *Exp Therm Fluid Sci* (2018) 96:101–10. doi:10.1016/j.expthermflusci.2018.03.004

17. Luan H, Weng L, Liu R, Li D, Wang M. Axial spacing effects on rotor-rotor interaction noise and vibration in a contra-rotating fan. *Int J Aerospace Eng* (2019) 2019:21259761–15. doi:10.1155/2019/2125976

18. Ai ZJ, Qin GL, Lin JX, Chen XF. Experimental study on the speed matching of two rotors for a counter-rotating fan. In: ASME Power Conference 2018; June 24-28, 2018; Lake Buena Vista, USA (2018). V002T09A001.

19. Joly M, Verstraete T, Paniagua G. Full design of a highly loaded and compact contra-rotating fan using multidisciplinary evolutionary optimization. In: Asme Turbo Expo 2013: Turbine Technical Conference & Exposition; June 3-7, 2013; San Antonio, USA (2013). p. GT2013–94433.

20. Cao LL, Watanabe S, Imanishi T, Yoshimura H, Furukawa A. Experimental analysis of flow structure in contra-rotating axial flow pump designed with different rotational speed concept. *J Therm Sci* (2013) 22(4):345–51. doi:10.1007/s11630-013-0634-x

21. Mohammadi A, Boroomand M. Design and internal flow analysis of a ducted contra-rotating axial flow fan. In: ASME 2014 International Mechanical Engineering Congress and Exposition; November 14-20, 2014; Montreal, Canada (2014). p. IMECE2014–39883.

22. Xu J, Tan C, Chen H, Zhu Y, Zhang D. Influence of tip clearance on performance of a contra-rotating fan. *J Therm Sci* (2009) 18(3):207–14. doi:10.1007/s11630-009-0207-1

23. Wang YG, Chen WX, Wu CH, Ren SY. Effects of tip clearance size on the performance and tip leakage vortex in dual-rows counter-rotating compressor. *P Mech Eng G-j Aer* (2015) 229(11):1953–65. doi:10.1177/0954410014562483

24. Grasso G, Moreau S, Christophe J, Schram C. Multi-disciplinary optimization of a contra-rotating fan. *Int J Aeroacoust* (2018) 17(6):655–86. doi:10.1177/1475472x18789000

25. Wang C, Huang LX. Passive noise reduction for a contra-rotating fan. *J Turbomach* (2015) 137(3):031007.1–10. doi:10.1115/1.4028357

## Nomenclature

$Q_v$ volume flow rate
$N_r$ shaft power
$n$ rotational speed
$P_{ref}$ reference sound pressure
$f_{r1}$ fundamental frequency of rotor 1
$f_{r2}$ fundamental frequency of rotor 2
$u_{rms}$ root mean square turbulence velocity
$k$ wave number
$\Lambda$ turbulence integral scale